Fluorenylporphyrins functionalized by electrochromic ruthenium units as redox-triggered fluorescence switches

Xu Zhang, Seifallah Abid, Limiao Shi, J. A. Gareth Williams, Mark A. Fox, Fabien Miomandre, Clarisse Tourbillon, Jean-Frédéric Audibert, Olivier Mongin, Frédéric Paul, et al.

Fluorenylporphyrins functionalized by Electrochromic Ruthenium Units as Redox-triggered Fluorescence Switches

Xu Zhang,[a,d] Seifallah Abid,[a] Limiao Shi,[a] J. A. Gareth Williams,[b] Mark A. Fox,[b,*] Fabien Miomandre,[c,*] Clarisse Tourbillon,[c] Jean-Frédéric Audibert,[c] Olivier Mongin,[a] Frédéric Paul,[a,*] Christine O. Paul-Roth,[a,*]

[a] *Univ Rennes, INSA Rennes, CNRS, ISCR (Institut des Sciences Chimiques de Rennes) – UMR 6226, F-35000 Rennes, France.*

[b] *Department of Chemistry, Durham University, Durham, DH1 3LE, U.K.*

[c] *PPSM, Ecole normale supérieure Paris-Saclay, 61 avenue du Président Wilson, 94235 Cachan, France*

[d] *Department of Chemistry, College of Chemistry and Chemical Engineering, Chifeng University, Chifeng, P. R. China*

Dedicated to Dr Jean-François Halet on his 60th Birthday

Abstract

Two dyads containing *tris*- and *tetrakis*-*meso*-fluorenyl-substituted porphyrin and ethynylruthenium units, **1** and **2**, were investigated by emission spectro-electrochemical (SEC) methods for their potential use as fluorescence switches. The ruthenium group as a potential electron donor and the porphyrin as a potential electron acceptor are connected by a phenylene bridge in **1** and by a fluorenylene bridge in **2**. The new fluorenyl-linked dyad **2** was probed by UV-visible, near-infrared (NIR) and infrared (IR) absorption SEC methods, and the properties interpreted with the aid of hybrid-DFT computations, for comparison with reported data for **1**. The porphyrin-based fluorescence of **1** decreased in intensity upon oxidation to $\mathbf{1}^+$ and decreased further on oxidising $\mathbf{1}^+$ to $\mathbf{1}^{2+}$. Negligible change in the fluorescence intensity of **2** was observed upon oxidation to $\mathbf{2}^+$ but the intensity decreased upon subsequent oxidation of $\mathbf{2}^+$ to $\mathbf{2}^{2+}$. These findings contrast with data reported for some other porphyrins appended with redox-active ruthenium or iron units, where fluorescence intensities increase upon oxidation of the peripheral metal centers, but they match data reported more recently for closely related arrays. A rationale for these apparently contrasting observations is proposed.

Keywords: *Porphyrin; Fluorene; Photoluminescence; Ruthenium Alkynyl Complex; Spectroelectrochemistry*

Graphical Abstract

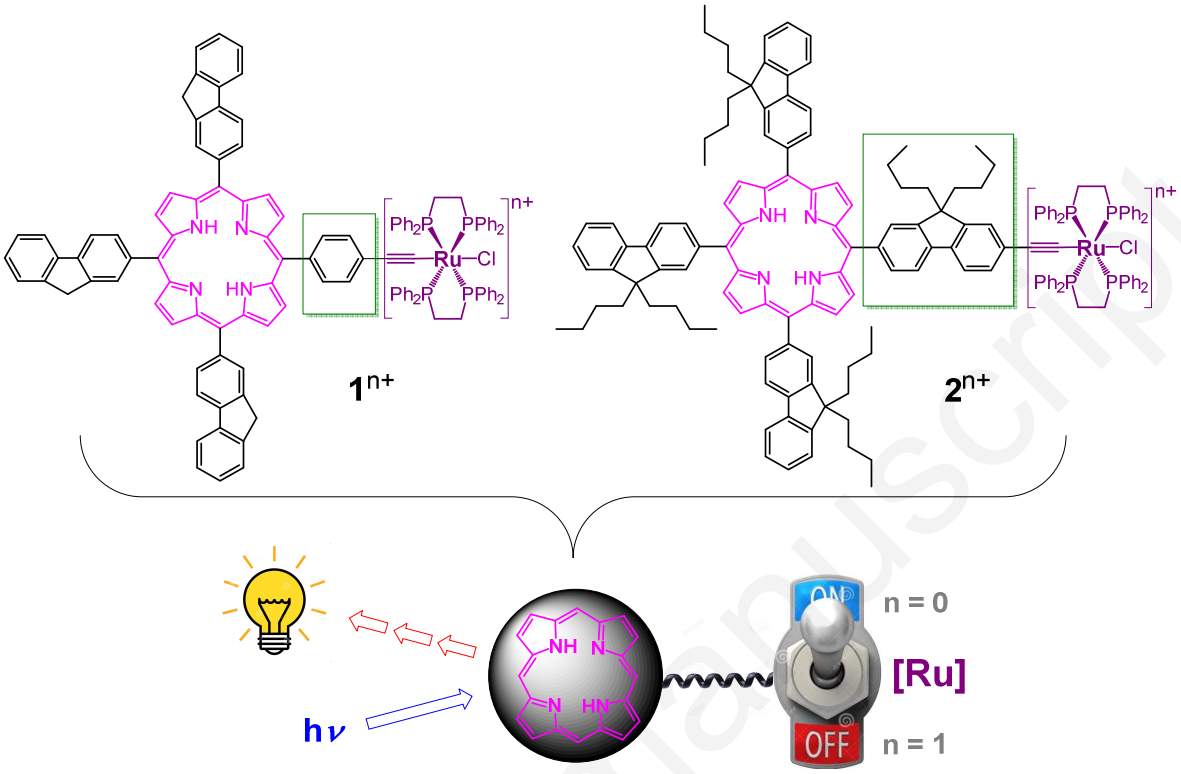

Fluorenylporphyrins functionalized by Electrochromic Ruthenium Units are used as Redox-triggered Fluorescence Switches.

Introduction

Porphyrin-based systems offer potential utility for efficient solar energy harvesting, owing to their strong absorption bands in selected regions of the spectrum. Several chromophores are needed in order to collect light from as wide a part of the solar spectrum as possible.[1,2] Thus, the ability to design and construct molecular architectures in which energy flow can be controlled and switched on and off constitutes a great challenge. In 2007, Pryce's group reported interesting redox-controlled switching of the fluorescence of zinc(II) *meso*-ferrocenyl porphyrin complexes.[3] For example, in complex **A**, a ferrocenyl unit is directly connected to a triphenyl-zinc(II) porphyrin *via* one *meso* position. The fluorescence of complex **A** is almost negligible, yet when oxidized to $\mathbf{A}^+$, the fluorescence quantum yield Φ increases to 0.6 % (λ_{max} = 610, 660 nm). The efficient off/on redox switching of fluorescence was achieved by exploiting the quenching of the porphyrin excited state by electron-transfer from the ferrocene, a process that can be "switched off", reversibly, by oxidation to the ferrocenium ion.

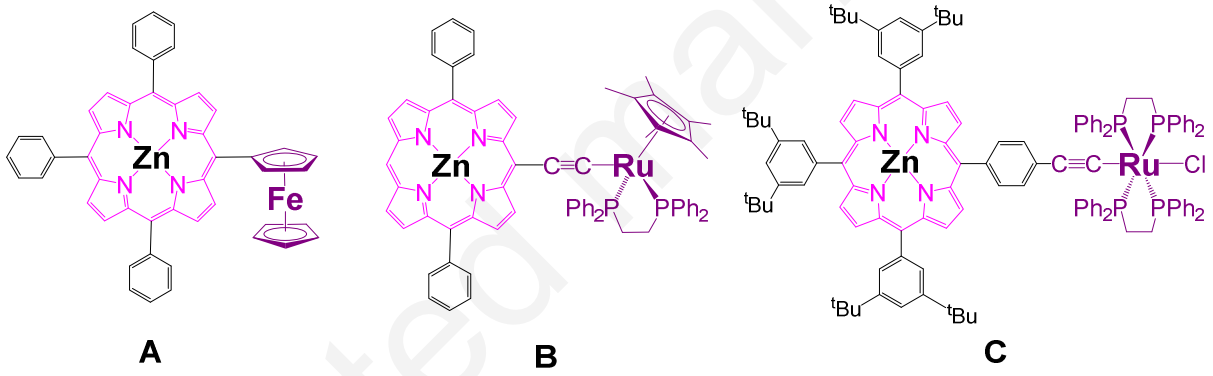

Figure 1. Previously reported fluorescence switches containing porphyrins.

In 2013, Akita and coworkers showed that the fluorescence of the ruthenium-appended porphyrin **B** could be redox-switched by oxidation/reduction between Ru(II) and Ru(III).[4] The fluorescence quantum yield of the neutral compound increases from 0.18 to 1.4 % upon oxidation to $\mathbf{B}^+$. We recently synthesized the dyad **1** (Figure 2), which has a ruthenium group as a potential electron donor and the porphyrin as a potential electron acceptor. The two parts are connected by an ethynylphenylene bridge.[5] Cyclic voltammetry (CV) and spectro-electrochemical (SEC) methods showed two stable oxidized species, $\mathbf{1}^+$ and $\mathbf{1}^{2+}$, and a stable reduced species $\mathbf{1}^-$. Complex **1** is therefore a potentially useful fluorescence switch although its fluorescence quantum yield is quite low (Φ_{lum} = 1.5%).[6] While this study was underway, one of us independently verified that the redox-modulation of luminescence can actually be effected using porphyrins functionalized by electroactive [*trans*-Ru(dppe)$_2$Cl(C≡C-)] or

[*trans*-Ru(dppe)$_2$(C≡CAr)(C≡C-)] units with dyad **C**, even when they present lower luminescence quantum yield in their than **1** Ru(II) state (Φ_{lum} ≈ 0.4 % for **C**).[7] In these systems, the redox switching of luminescence operates in a reverse way to that reported for the dyads **A** and **B**.[8] Based on our experience with tetrafluorenylporphyrins,[9-12] the new dyad **2** was then targeted, in which the 1,4-phenylene linker is replaced by a 2,7-fluorenylene linker, with the expectation that this extended linker would slow down the rate of the photo-induced electron transfer at the origin of the low luminescence quantum yield in the Ru(II) state,[12] and would therefore show a more contrasted redox-switching compared to **1** (and **C**).

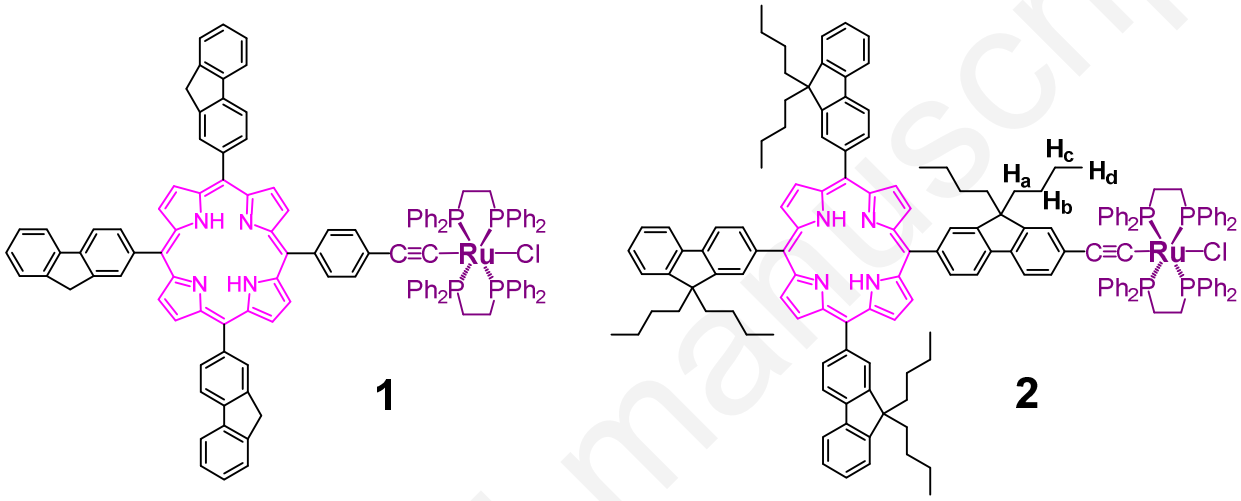

Figure 2. Fluorescence switches **1** and **2** explored in this study.

The results of a fluorochromic study conducted on **1** and **2** using spectroelectrochemistry are now reported. Firstly, the synthetic, photophysical, electrochemical and spectro-electrochemical data for the new dyad **2** are described, together with supporting computational results. Secondly, the fluorescence on-off switching properties of the dyads **1** and **2** are reported, revealing an unexpected behavior. Finally, these results will be discussed and rationalized in the light of the available data from **A**-**C** and from isoelectronic Fe(II) and Ru(II) alkynyl complexes.[13,14,15]

Synthesis and characterization of new dyad 2

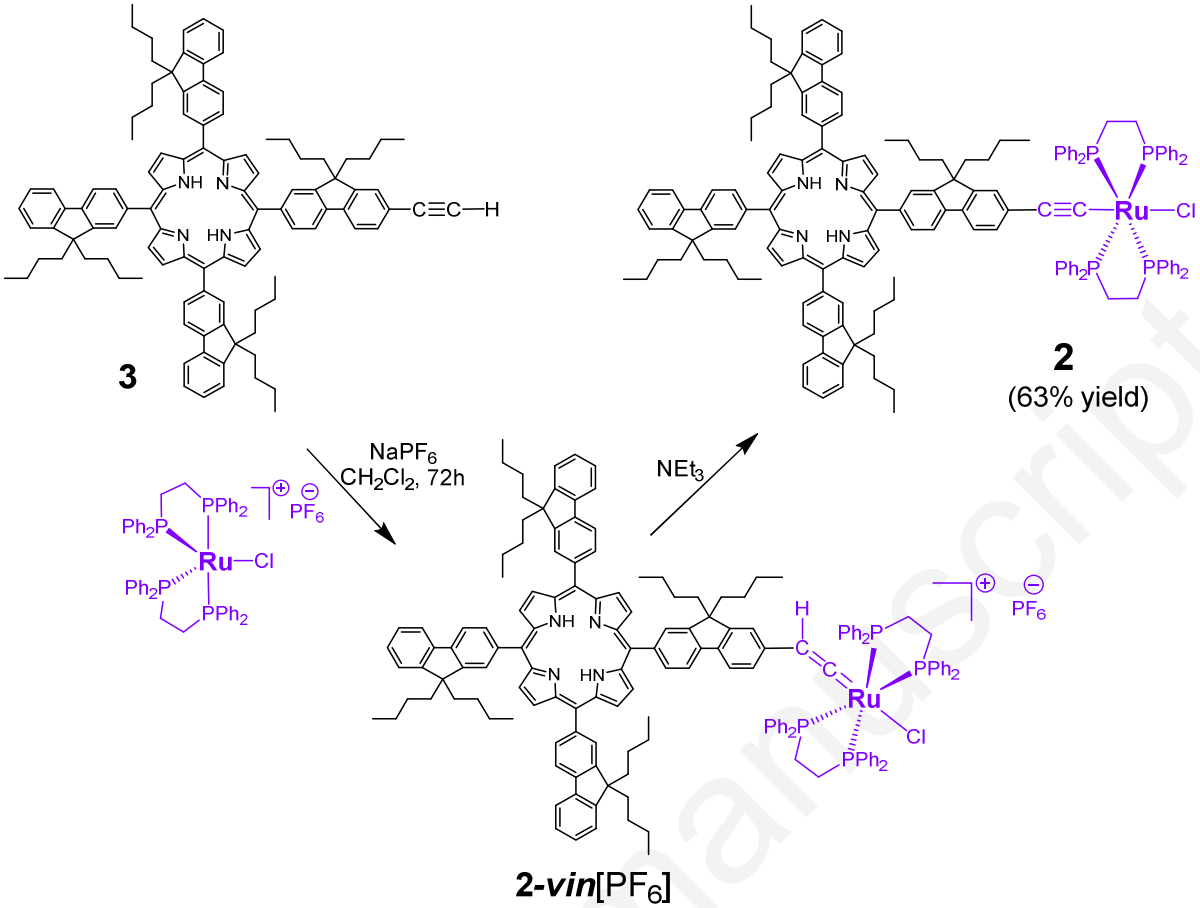

Scheme 1. Synthesis of **2**.

As shown in Scheme 1, the desired organometallic compound **2** can be synthesized from porphyrin **3**[16] and the ruthenium salt *cis*-[RuCl(dppe)$_2$][PF$_6$] in two steps via the vinylidene intermediate **2-*vin***[PF$_6$] in good yield.[17] The reaction mixture was stirred at room temperature and its progress was followed by ^{31}P and ^{1}H NMR spectroscopy. The 16-electron complex, *cis*-[RuCl(dppe)$_2$][PF$_6$], is characterized by two triplets at 55.8 and 83.7 ppm in the ^{31}P{^{1}H} NMR spectrum, whereas the intermediate **2-*vin***[PF$_6$] formed has a singlet at around 37 ppm. The ^{1}H NMR shows the completion of the reaction as the singlet of the terminal alkyne at 3.3 ppm disappears after 72 h. The base, NEt$_3$, was added dropwise under argon to convert the vinylidene **2-*vin***[PF$_6$] into the desired alkynylruthenium product **2**. After purification, this new complex was characterized by ^{1}H and ^{31}P NMR spectroscopy and high-resolution mass spectrometry (Figures S1-S4).

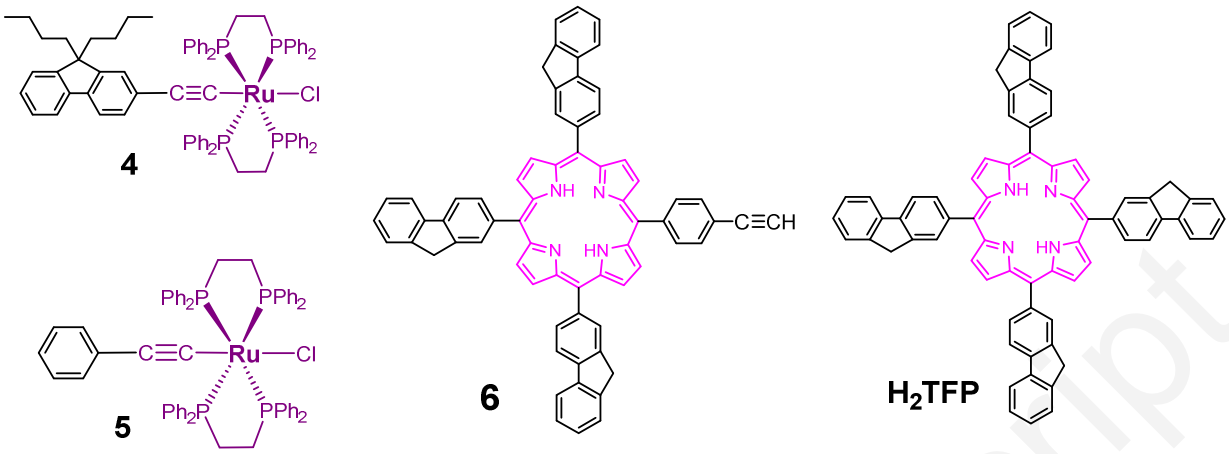

Figure 3. Compounds used as references for this study.

Photophysical properties

The UV-visible absorption spectrum of **2** exhibits features that are typical of free-base porphyrins: an intense Soret bands around 427 nm and four Q-bands in the visible region (ESI; Figure S4 and Table S1). Comparison of the UV-visible spectra of **2** and **3** indicates that bands associated with the ruthenium unit in **2** are much weaker than those of the porphyrin, with the only apparent additional bands being centered around 370 nm, probably attributable to d(Ru) $\rightarrow$ π^*(C≡C) metal-to-ligand charge-transfer (MLCT). A similar band is found at 373 nm in **4**.[13] The fluorescence spectra for **2** and **3** are similar in toluene with two Q bands at *ca.* 659 and 724 nm for **2'** (Figures S5-S6). This spectra is also nearly identical to that of porphyrin **1**.[5] A quantum yield of 20% was measured for **3**, whilst, contrary to our expectations, there is essentially no emission from **2** (Φ_{lum} < 0.5%).[18]

Electrochemistry and spectroelectrochemistry

The cyclic voltammogram of **2** is very similar to that of **1** (Figure S7).[5] It reveals a reversible first oxidation wave at -0.04 V (Table 1), in addition to the expected oxidation and reduction waves attributed to the porphyrin units.[20,9,21] This wave is due to oxidation at the ruthenium ethynyl unit at a quite similar potential to the ferrocenium/ferrocene couple.[22,23] For comparison, Ru(dppe)$_2$(C≡CFl)Cl **4** has an oxidation potential of -0.02 V.[14] These values

show that the tetrafluorenylporphyrin moiety has a negligible effect on the oxidation of the ruthenium ethynyl unit in **2**.

Table 1: Cyclic voltammetry data for complexes **1** and **2** in CH_2Cl_2. Half wave potentials are quoted with reference to the ferrocenium/ ferrocene couple at 0 V. [a]

	E_{Ru}	E_{Ox1}	E_{Ox2}	E_{Red1}	Ref
1	-0.02	0.48	*0.81*	-1.70	This work
2	-0.04	0.53	*0.87*	-1.67	This work
4	-0.02[b]	/	/	/	This work
5	0.01[b]	/	/	/	This work
6	/	0.53	0.82	-1.65	[5]
H_2TFP	/	0.58	0.90	/	[19]

[a] Values in italics are potentials of irreversible waves. [b] Differences with values previously measured[13] for **4** and **5** result from the slightly different electrode potential presently considered for referencing (see Experimental Part).

Spectroelectrochemistry (SEC) measurements were then carried out on complex **2**, to obtain the absorption spectra (Figure S8) and establish the stability of the oxidized species $\mathbf{2}^+$ prior to SEC emission measurements. The first oxidation process for **2** was reversible in the SEC cell based on UV-Vis-NIR spectra: the neutral species was re-formed on back reduction of the oxidized monocation $\mathbf{2}^+$. Absorption measurements of the oxidized species for both ruthenium-porphyrin complexes **1** and **2** are listed in Table S1 for comparison.[5] The near-IR (NIR) spectrum for the first oxidized species of the ruthenium complex **2** contains a weak band at around 11210 cm^{-1} with a shoulder at 8500 cm^{-1} (Figure S8 inset and Table S2: 892 and 1176 nm, respectively). Such bands are characteristic of the fluorenylethynylruthenium moiety on oxidation.[13,14] Thus, the absorption spectra of $\mathbf{2}^{n+}$ (n = 0, 1) is merely the sum of those of **3** and $\mathbf{4}^{n+}$ in each redox state (ESI; Figures S10a-b). A similar statement can be made for the spectrum of $\mathbf{1}^{n+}$ when compared to those of **6** and $\mathbf{5}^{n+}$ (Figures S11a-b), in line with a weak electronic coupling between the organoruthenium endgroup and the porphyrin ring in both dyads, regardless of its oxidation state. Furthermore, from the spectroscopic data obtained for $\mathbf{1}^{2+}$ and $\mathbf{6}^+$ (Figure S4), we can infer that the dicationic molecule $\mathbf{1}^{2+}$ corresponds to a diradical state with one unpaired electron on the oxidized porphyrin ring and the other on the appended Ru(III) center.

IR spectroelectrochemistry was also carried out on dyad **2** (Figure S9 and Table S2). On oxidation, the C≡C band corresponding to the neutral species disappeared and a strong C≡C

band at 1916 cm^{-1} appeared. The energy difference of 148 cm^{-1} for these C≡C bands on oxidation is typical of arylethynylruthenium complexes.[8,24] This confirms that the porphyrin unit has little influence on the spectral properties associated with the Ru unit in **2** and may be considered as a spectator as had already been found for **1**.

Computations

A geometry optimization on a model molecule of **2**, where the butyl groups were replaced by hydrogen atoms (**2′**), was carried out with the hybrid-DFT functional B3LYP.[25] This functional was previously used for computing the electronic structure of the corresponding model of **1** (**1′**).[5] Calculations on the model geometry **2′** reveal HOMO, HOMO-1 and HOMO-2 with similar energies of -4.57, -4.85 and -4.88 eV mainly located at the ethynylruthenium unit whereas the degenerate LUMO and LUMO+1 are on the porphyrin unit (Figure 4 and ESI;Table S3). While the LUMO is essentially located on the porphyrin only, the porphyrin contributes little (5%) to the HOMO. The HOMO being where the electron is considered to be lost on oxidation, the latter can be considered to be taking place at the ethynylruthenium unit, in line with CV data. For comparison, the porphyrin unit contributes 29% to the HOMO in **1** which suggests that the porphyrin in **2** has much less influence on the oxidation process of **2** than the porphyrin unit in **1** in that of **1**.[5] This observation would be consistent with a higher degree of electronic coupling between the porphyrin ring and the Ru(II) center in **1** than in **2**.

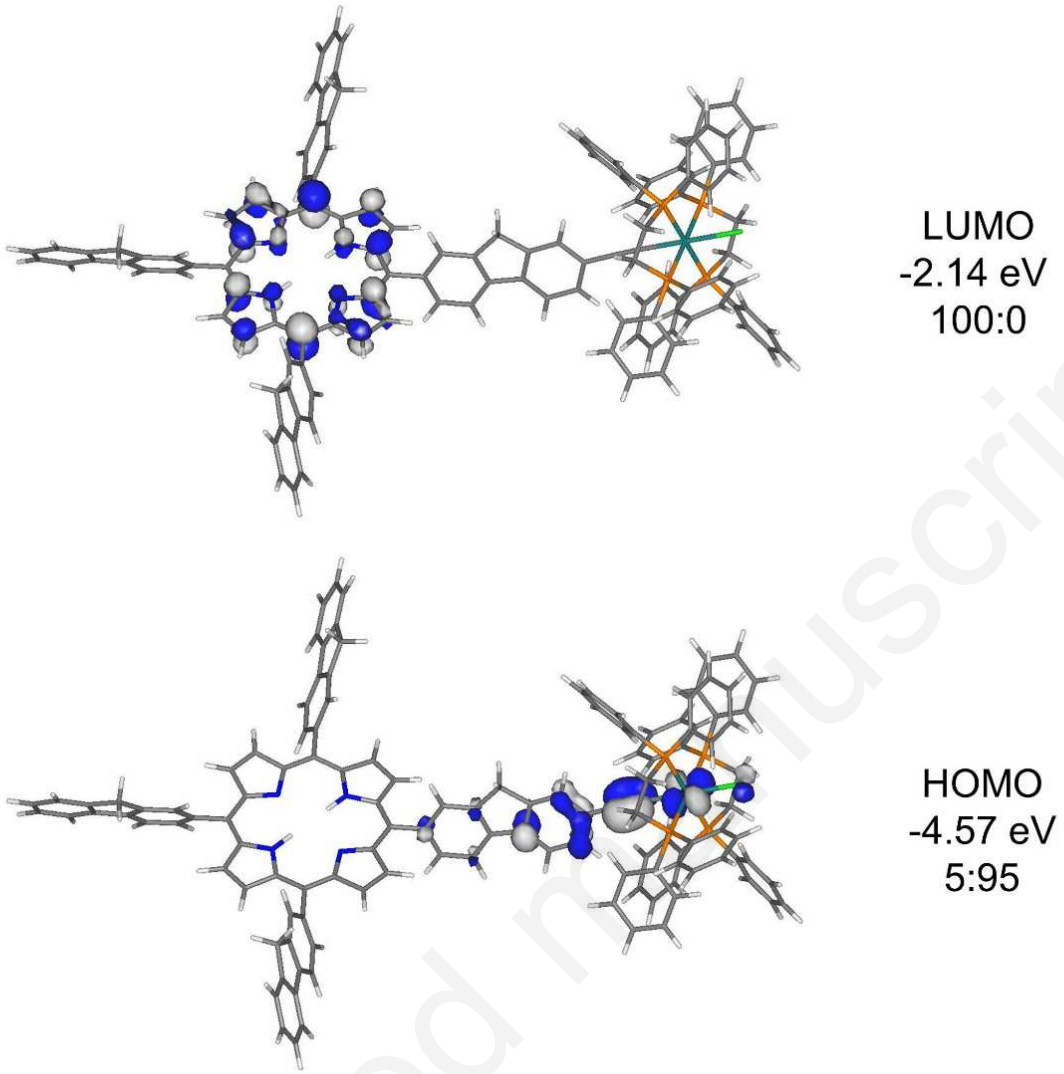

Figure 4. Frontier molecular orbitals for the optimized model geometry **2'** at B3LYP. The ratios correspond to % orbital contributions on the porphyrin and $[C_{13}H_8C{\equiv}CRu(dppe)_2Cl]$ fragments.

Among the singlet state transitions from TD-DFT data for both complexes at B3LYP (Table S4), the $Q_x[0,0]$, $Q_y[0,0]$ and Soret (B) bands could be identified each time among the most intense allowed transitions found (Figure S13). A significant amount of MLCT character was present in the Q-bands and many other porphyrin based-transitions of **1′** and **2′**. Attempts to identify a MLCT transition at lower energies for both systems, potentially corresponding to a (vertical) transition into the charge-separated (CS) state responsible for the photo-induced redox quenching process discussed below were unsuccessful. While MLCT character is apparent in all the lowest-lying singlet transitions (including the Q-bands), most of them have a multi-configurational nature and exhibit weak to negligible oscillator strengths. Most likely, such a transition is forbidden or very weakly allowed. TD-DFT computations at B3LYP were also performed on **1′** and **2′** for triplet states to explore the possibility of intersystem crossing

(ISC) taking place. The lowest transitions from the ground state (S_0) to the first triplet excited state (T_1 and T_2) are predicted to be at 903 and 751 nm for **1′** and at 994 and 738 nm for **2′**. In terms of the nature of transitions, these triplet states resemble the two first singlet states (S_1 and S_2).[25, 26]

Electrofluorochromism

As mentioned above, compounds **1** and **2** show quite similar emission spectra. Our interest is to investigate whether the emission intensity can be monitored electrochemically, especially upon oxidation.

A first experiment consisted in using a thin layer spectroelectrochemical cell coupled to a spectrofluorimeter to record the voltafluorogram of **1**. Figure 5 shows the variation of fluorescence intensity at 660 nm when the potential is scanned linearly from 0 to 1.4 V and back to 0 V.[27] The results clearly indicate that fluorescence of **1** is partly quenched as soon as the first oxidation occurs. A continuous decrease in fluorescence intensity is observed as the potential is scanned anodically. Scanning the potential in the opposite direction stops the quenching and the fluorescence increases when the reduction of $\mathbf{1}^+$ occurs at the end of the backward scan.

To confirm and further analyze this behavior, similar experiments were performed using a set-up built in-house that couples electrochemistry and epifluorescence microscopy. In this case, potential steps are applied to initial (0.5 V), mono-oxidized (1.0 V) and di-oxidized (1.5 V) species (see Figure S17a for the corresponding CV and location of the selected potential values).[27] A clear and (quasi-)reversible modulation of fluorescence intensity for the main emission band (660 nm) can be seen in both cases (Figure 6). The most striking feature is that the amplitude of the modulation is significantly different for both compounds, especially as far as the first oxidation is concerned: indeed, it is much larger for compound **1** than for compound **2**. In any case, the modulation goes deeper when the potential is switched to a more positive value, and the process is reversible, although the initial fluorescence intensity is not fully recovered. It can be noticed that applying a potential step from open circuit (o. c.) to 0 V does not change the fluorescence intensity at all, showing that a change in the redox state is actually required. A slight modulation is observed when the potential is switched from o. c. to 0.5 V which corresponds to the foot of the first oxidation

wave, but the fluorescence switching becomes really significant when the potential is pushed to 1 V or 1.5 V, where an exhaustive redox state change occurs.

The first oxidation step (from o. c. to 1 V) clearly involves the oxidation of the Ru center as discussed above. Similarly to dyad **C**,[7] oxidizing the Ru center does not enhance the fluorescence as in previously reported systems,[3,4] but conversely leads to further quenching. It is worth mentioning the role played by the linker between the metal and the porphyrin core in this process: substituting the phenyl by a fluorenyl linker clearly restricts the quenching process (Figure 7A). As far as the second oxidation is concerned, in both cases a large fluorescence quenching occurs with an amplitude which is also larger for **1** than for **2** (Figure 7B), but with a smaller difference between both compared to the first oxidation. This second oxidation step concerns the porphyrin moiety which is also the fluorophore.

The analysis of how emission spectra vary upon oxidation shows no modification except perhaps the relative intensity of the two main bands. Interestingly the same features in the fluorescence modulation are qualitatively observed whatever the emission wavelength chosen (Figure S18). Based on that statement, we believe that both neutral and mono-oxidized parents of $\mathbf{1}^{n+}$ and $\mathbf{2}^{n+}$ have nearly the same emission spectrum, in line with the weak electronic coupling between the emissive porphyrin ring and the redox-active organoruthenium endgroup previously evidenced. As a result, the two halves of these dyads present essentially the same electronic signatures as the model compounds, mimicking them and taken in the correct redox state. Then, as regard the second oxidation, we believe that the corresponding dicationic species are essentially non-emissive in the investigated spectral range and so only contribute to decrease the overall luminescence at potentials at which such species are formed. [28,29]

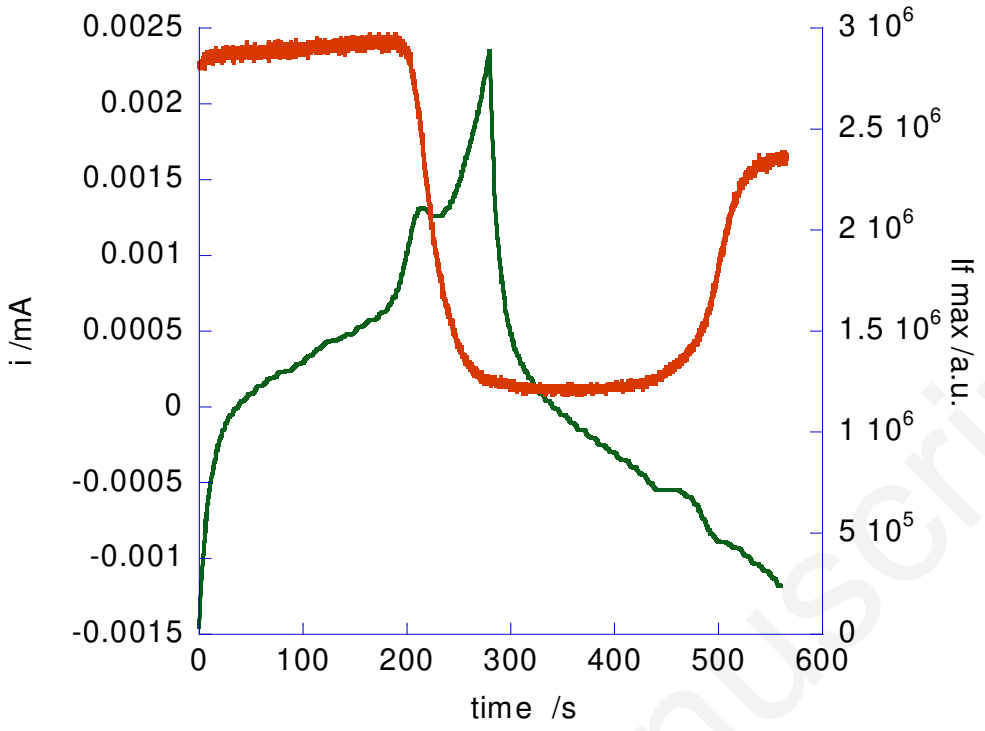

Figure 5. Fluorescence intensity (red trace, right scale) and electrochemical current (green trace, left scale) for **1** in CH_2Cl_2 / $[NBu_4][PF_6]$ (0.1 M) as functions of time upon potential linear scan from 0 V to 1.4 V and back to 0 V (scan rate : 2 mV/s). Recorded in a thin layer spectroelectrochemical cell coupled to a spectrofluorimeter (excitation 420 nm).

In the studies of related dyes in which a redox-active (organometallic) endgroup is connected to a porphyrin, electron- and energy-transfer processes are often put forward to rationalize the changes in luminescence relative to the unsubstituted reference porphyrin.[3,4,7,30] To investigate further the mechanism involved in the electrofluorochromic behavior of **1**, UV-vis absorption spectroelectrochemistry was performed in a thin layer cell and the spectral changes were plotted on a differential scale to better evidence them (ESI; Figure S19). As already stated,[5] Ru(II) oxidation leads to very weak changes. However, when pushing the potential toward more positive values, a dramatic drop in the Soret absorption band is observed with the appearance of a weak band centered at 470 nm, along with another band in the red part of the spectrum, near 700 nm, indicating the *in situ* formation at the electrode of the corresponding dications featuring an oxidized porphyrin. While the Ru(II) oxidation does not appear to "switch on" a strong absorption in the emission range of the lowest porphyrin-based singlet states, a careful comparison of the emission spectrum of **3** and **6**, taken to model the porphyrin-based emission in $\mathbf{2}^{n+}$ and $\mathbf{1}^{n+}$ (n = 0, 1), with the absorption spectra of $\mathbf{4}^{n+}$ and

$\mathbf{5}^{n+}$, taken to model the absorption of the Ru(II)/Ru(III) organometallic part of these dyads, reveals that there is a slight but non-negligible spectral overlap between the emission of **3** and **6** and the absorptions of $\mathbf{4}^{+}$ and $\mathbf{5}^{+}$ (Figures S20a-b). In contrast, the comparison between the emission of **3** and **6** and the absorptions of **4** and **5** confirms the total absence of spectral overlap. Thus, the participation of an energy transfer process in the luminescence quenching process can be strictly excluded for the neutral dyads, not for the monocations $\mathbf{1}^{+}$ and $\mathbf{2}^{+}$.

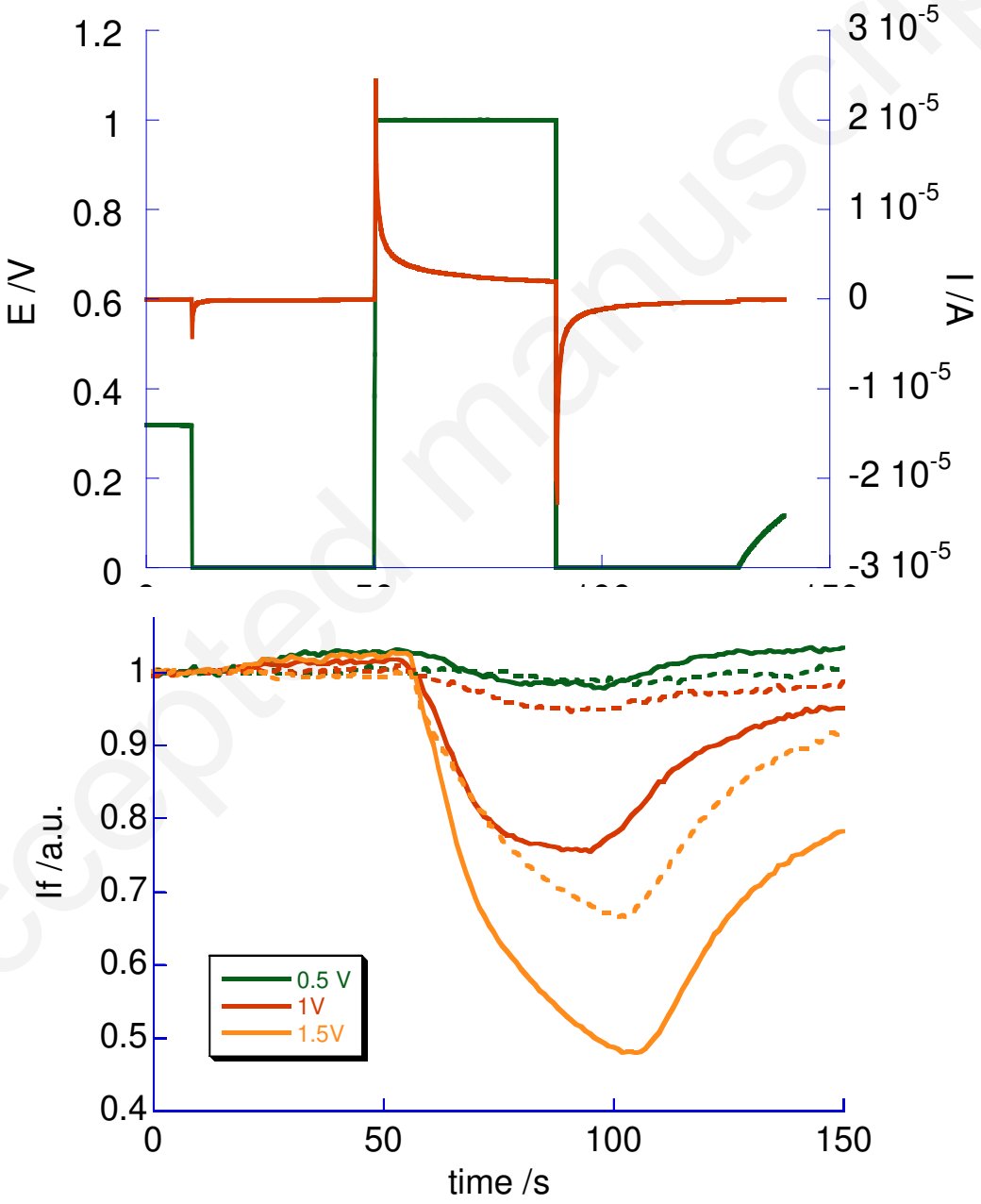

Figure 6. Normalized emission intensity recorded at 660 nm (excitation 447 nm) in CH_2Cl_2 / $[NBu_4][PF_6]$ (0.1 M) upon potential steps from 0 to the indicated values for compound **1** (full line) and **2** (dashed line). The potential signal and corresponding electrochemical current are shown in the top panel for 1 V and compound **1**.

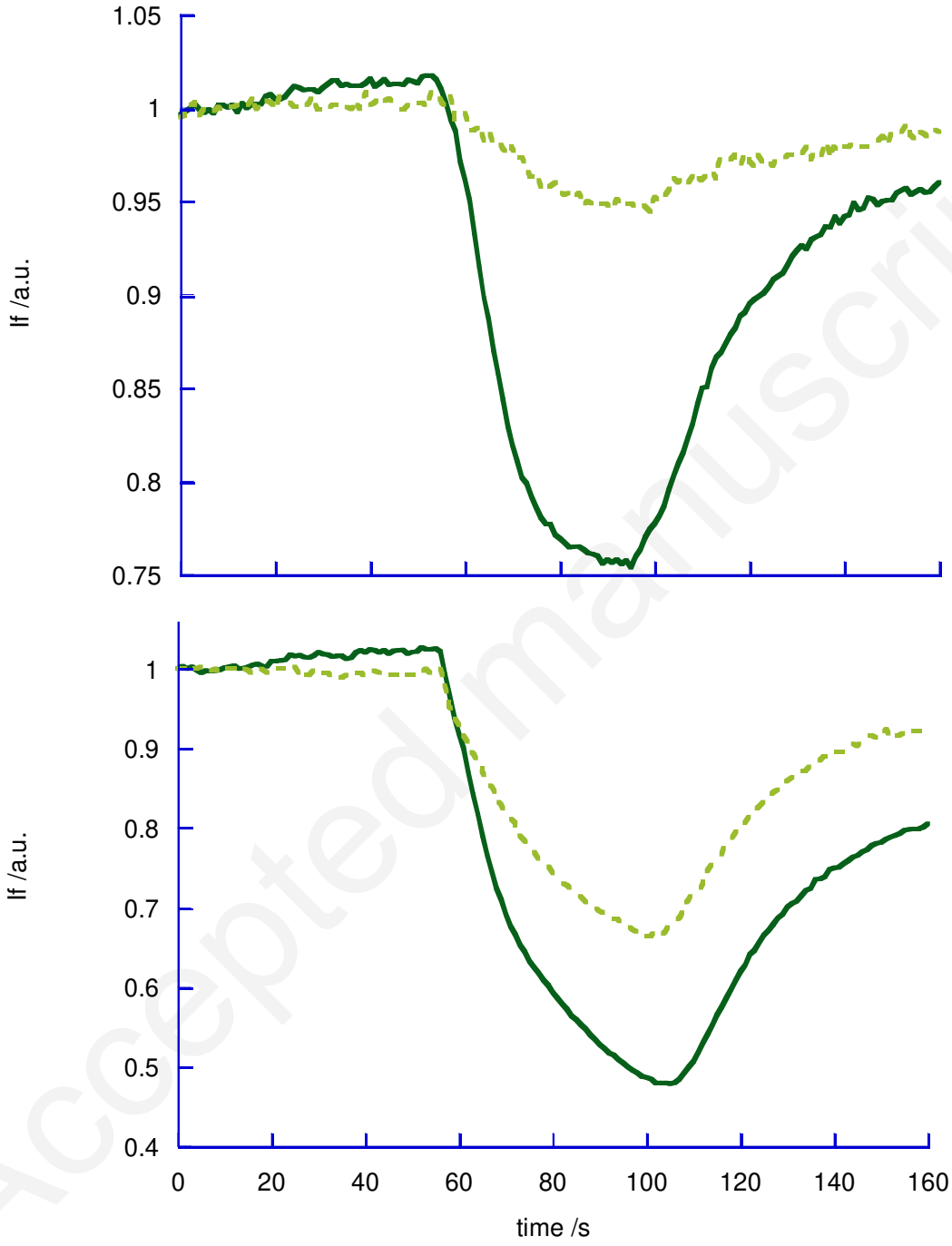

Figure 7. Comparison of normalized emission intensity recorded at 660 nm (excitation 447 nm) in CH_2Cl_2 / $[NBu_4][PF_6]$ (0.1 M) upon potential steps from 0 to 1 V (top) or 1.5 V (bottom) for compound **1** (full line) and **2** (dashed line).

Photoinduced Intramolecular Electron-transfer in the Neutral and Monocationic State for 1 and 2

In order to learn more about the potential participation of electron-transfer reactions in the luminescence quenching process, we have analyzed the energetics associated with redox-trapping of the Q_x-state as given by the Rehm-Weller[31] and Marcus[32,33] equations for the neutral and monocationic dyads. Estimates of the free enthalpy of formation (ΔG_{CS}) of the intramolecular charge-separated state corresponding to the formal transfer of one electron from M(II) toward the fluorenyl ligand (CS) can be derived for **1** and **2** using eq. 1 (Table 2).[34] The (vertical) energy of this CT state can also be estimated by adding the reorganization energy of the redox sites to ΔG_{CS}. The driving force (ΔG_{eT}) and the activation energy ($\Delta G^{\neq}$) for the electron transfer can then be derived according to eq. 2 (Scheme 2A).[35] A mean reorganization of 0.9 eV was considered when deriving these figures,[13] given that the reorganization of the Ru complex is usually around 0.8-0.9 eV.[36,37]

$$\Delta G_{CS} = E°(Ru^{II}/Ru^{III+}) - E°(Por/Por^{-}) + (Z_P - Z_{Ru} - 1)e^2/(4\pi\varepsilon_0\varepsilon d) \qquad (1)$$

$$\Delta G^{\neq} = (\Delta G_{eT} + \lambda)^2/(4\lambda) \qquad (2)$$

Table 2: Thermodynamic figures derived for the reductive trapping of the emissive state of **1** or **2** in the lowest charge transfer (CS) state (Rehm-Weller).

	$E°_{Ru}$ [a]	$E°_{Por}$ [a]	$\Delta E°$ [b]	$d_{Ru\text{-}P}$(Å) [c]	ΔG_{CS} [d]	λ_{CS}(nm) [e]	ΔG_{eT} [f]	$\Delta G^{\neq\uparrow}$ [g]
1	-0.02	-1.70	1.68	12.3	1.55	506	-0.36	0.081
2	-0.04	-1.67	1.63	16.4	1.53	510	-0.38	0.076

[a] All E° values given for redox couples are in V vs. FcH^+/FcH. Conditions (unless stated otherwise): CH_2Cl_2 solvent, 0.1 M $[NBu_4][PF_6]$ supporting electrolyte, 20°C, Pt electrode, sweep rate 0.1 V s^{-1}. [b] Difference between previous first oxidation and reduction potentials. [c] Ru-porphyrin distance derived from available X-ray data.[13,38] [d] Computed (in eV) according to eq. 1 (see text). [e] Wavelength of the vertical transition to the CS state responsible for the trapping considering a reorganization energy of 0.9 eV for the electron transfer process. [f] Driving force (in eV) for the electron transfer step. [g] Activation energy (in eV) for the electron-transfer step computed for a reorganization energy of 0.9 eV (eq. 2).

Estimates of the free enthalpy of formation (ΔG_{CT}) of the intramolecular charge-transfer state corresponding to the formal transfer of one electron from the porphyrin to the Ru(III) center (CT) were also derived for **1**$[PF_6]$ and **2**$[PF_6]$ (Table 3 and Scheme 2B) using a

simplified version of eq. 1 (eq. 3). These ΔG_{CT} values are given by the difference between the first oxidation potential of the porphyrin ligand obtained from **6** or **H_2TFP** (Table 1) and the metal-based reduction potential of the Ru(III) center obtained from $\mathbf{1}^+$ and $\mathbf{2}^+$. Despite the approximations made in eqs 1 and 5 (notably the neglect of the electron-electron correlation energy), a fair match is found between the vertical transition energy to this CT state and the maximum of the LMCT absorption of **1** and **2** (Table 3).[39]

$$\Delta G_{CS} = E°(Por/Por^+) - E°(Ru^{III}/Ru^{II}) \qquad (3)$$

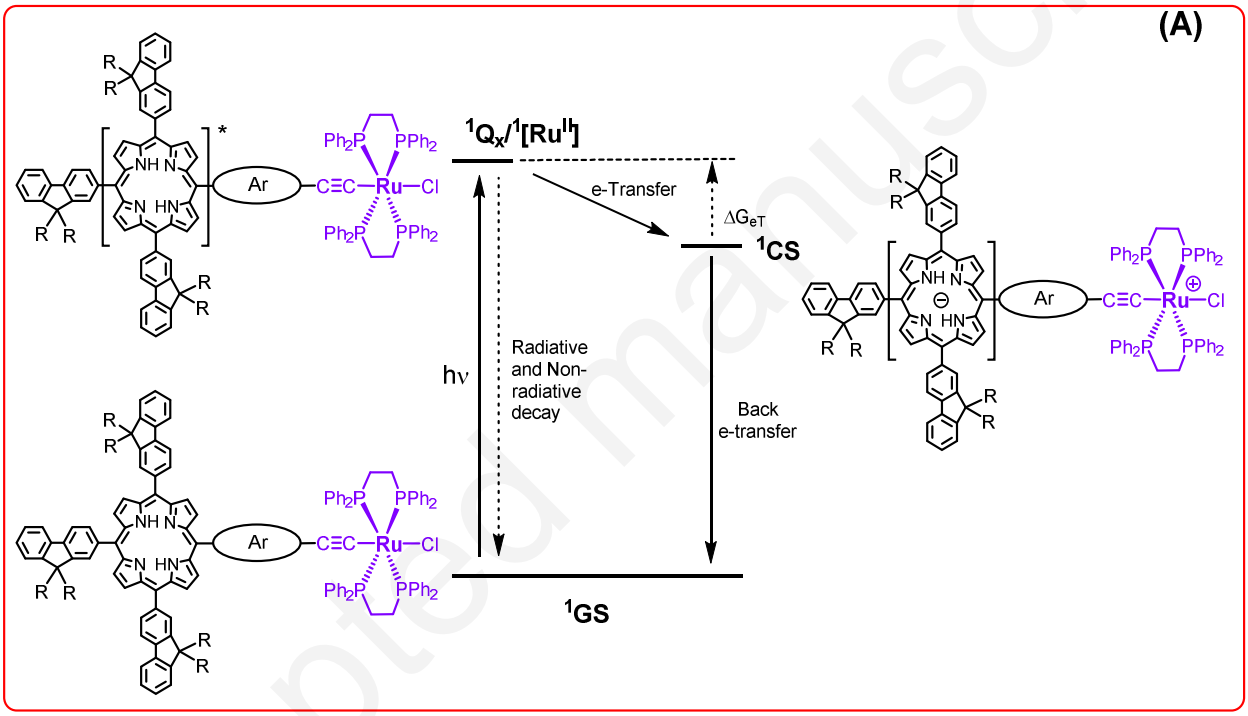

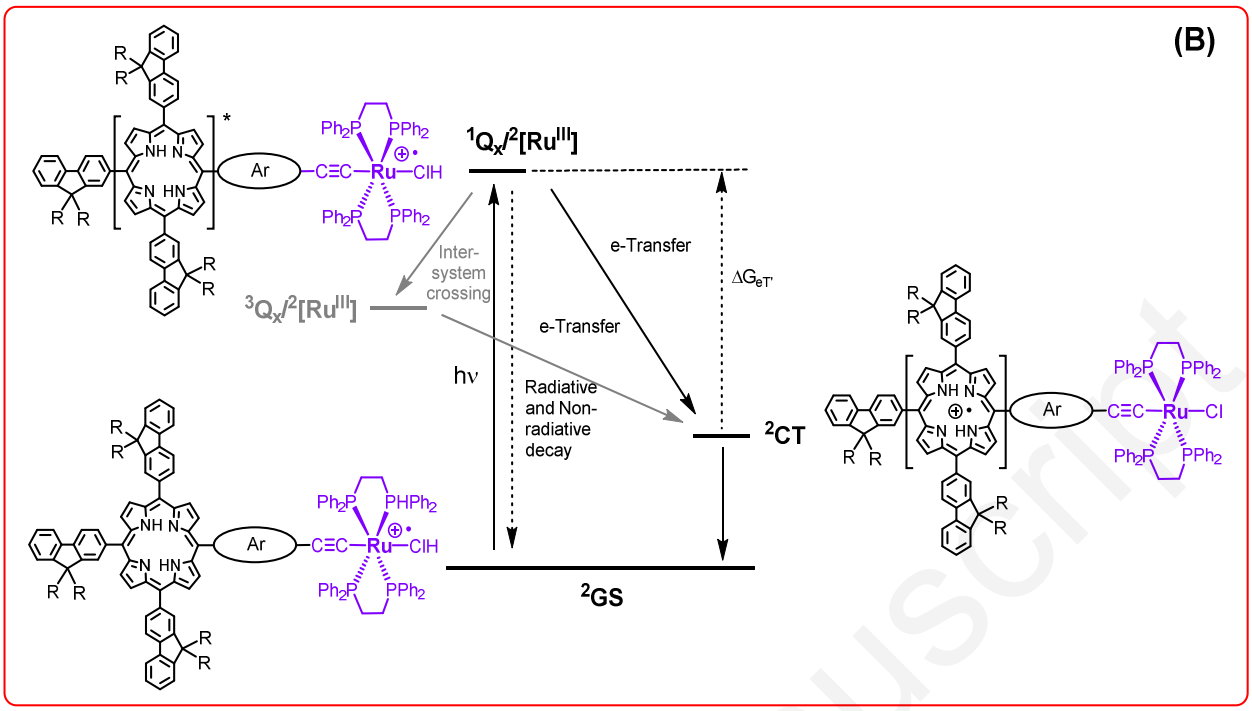

Scheme 2. Luminescence-quenching mechanisms by electron-transfer for Dyads **1** and **2** in their neutral (A) and monocationic (B) redox states.

Table 3: Thermodynamic figures derived for the reductive trapping of the emissive state of $\mathbf{1}^+$ or $\mathbf{2}^+$ in the lowest charge transfer (CT) state (Rehm-Weller).

	$E°_{Ru}$ [a]	$E°_{Por}$ [a]	$\Delta E°$ [b]	ΔG_{CT} [c]	λ_{CT}(nm) [d]	ΔG_{eT} [e]	$\Delta G^{\neq}$ [f]
$\mathbf{1}^+$	-0.02	0.53	0.55	0.55	855	-1.36	0.058
$\mathbf{2}^+$	-0.04	0.58	0.62	0.62	843	-1.29	0.042

[a] All E° values given for redox couples are in V vs. FcH^+/FcH. Conditions (unless stated otherwise): CH_2Cl_2 solvent, 0.1 M $[NBu_4][PF_6]$ supporting electrolyte, 20 °C, Pt electrode, sweep rate 0.1 V s^{-1}. [b] Difference between previous peak potentials. [c] Computed (in eV) according to eq. 3 (see text). [d] Wavelength of the vertical transition to the CT state responsible for the trapping. [e] Driving force (in eV) for the electron transfer step. [f] Activation energy (in eV) for the electron-transfer step computed for a reorganization energy of 0.9 eV (eq. 2).

All these excited state-trapping reactions are energetically downhill (ΔG_{eT} or $\Delta G_{eT'}$ < 0), in line with their relevance to the luminescence-quenching process. These reactions are supposed to take place with a rate given by eq. 4 and corresponding to a non-adiabatic

electron transfer.[33,40] Based on the activation energies ($\Delta H^{\neq}$) and provided the electronic coupling (H_{ab}) does not change too much for a given dyad upon oxidation, faster quenching of the emitting state by energy transfer into the charge-separated state should occur for the cations **1**[PF_6] and **2**[PF_6] than for their neutral parents **1** and **2**. Thus, a photo-induced electron-transfer quenching processes could (at least qualitatively) explain the redox-switching of luminescence experimentally observed. However, considering that the values found for the activation energy ($\Delta H^{\neq}$) are subject to uncertainties,[41] some caution when rationalizing the experimental observations by redox-trapping only is thus required.[42] The main finding from this section is therefore that the redox-quenching processes occurring in the neutral and in the mono-oxidized state of one of these dyads should impact the luminescence quantum yield with fairly close efficiencies.

$$k_{eT} = C(H_{ab})^2 \exp(-\Delta G^{\neq}/k_B T) \qquad (4)$$

Note also that activation energies are presently much better suited than exergonicities (ΔG_{eT}) to compare the rates of these reactions, because the electron transfer actually occurs in the inverted Marcus region for the mono-oxidized dyads $\mathbf{1}^+$ and $\mathbf{2}^+$. In this respect, as indicated on Scheme 2B, redox-trapping into the CT state might also occur from a porphyrin-based (triplet) state at lower energy, in spite of the lesser exergonicity of such a reaction.[30,43,44]

Discussion

Electronic coupling in 1 vs. 2

In line with the conclusions drawn from the CV data (Table 1) and from the IR SEC data (Table S9), the UV-vis absorption data gathered for the dyads **1** and **2** and for the reference compounds **5**-**6** and **3**-**4** in their various redox states (Figures S10-S12) suggest that the porphyrin core and the ruthenium alkynyl complex are not strongly coupled in these dyads in all redox states considered. Similar observations have already been reported in the literature for other dyads containing *meso*-tetra-arylporphyrins connected via their peripheral *para*-phenyl positions.[45] DFT calculations further suggest a significantly smaller electronic coupling for **2** compared to **1**. These sub-units can therefore be considered as presenting the same spectral signatures as the chromophores/luminophores constituting the dyad but taken

independently. Under such conditions the similarity of the porphyrin-based emission for a given dyad in its first two redox states ($\mathbf{1}^{n+}$ or $\mathbf{2}^{n+}$, n = 0,1) is not surprising.[3, 7]

Luminescence quenching processes in 1 and 2

The static luminescence quantum yield (Φ_{lum}) measured for an emissive site in a dyad where several competitive processes contribute to quench its luminescence corresponds in principle to the following fraction (eq. 5),[14] in which k_{lum} represents the fluorescence decay rate of that site, k_{eT} the electron transfer rate, k_{ET} the energy transfer rate and k_{NR} the sum all other non-radiative decay processes (internal conversion, intersystem crossing, etc…).

$$\Phi_{lum} = k_{lum}/(k_{lum} + k_{eT} + k_{EnT} + k_{NR}) \qquad (5)$$

Before discussing further the origin of the present redox-switching of fluorescence in $\mathbf{1}^{n+}$ and $\mathbf{2}^{n+}$ (n = 0, 1, 2), the various mechanisms by which the non-radiative decay can take place in a given redox state for these compounds will be analyzed. Among these, intersystem crossing to the triplet state (presently included in k_{NR} in eq. 5) will certainly contribute to quench the fluorescence of the emitting state, especially given the presence of the heavy ruthenium atom.[30] However, given that this process should remain fairly constant for **1** and **2** irrespective of their redox state, we expect it not to contribute to the redox-induced modulation of fluorescence for these dyads.

Neutral Compounds. We have recently shown that the first (triplet) ligand field states (^{3}LF) for [*trans*-Ru(dppe)$_2$Cl(C≡CAr)] (Ar = 3- and 4-(9,9'-dibutyl-2-fluorenyl)phenyl) metal alkynyl complexes are located *ca.* 2.2 eV above the ground state.[13] Thus, with the emissive (Q_x) state presenting a $\lambda_{0\text{-}0}$ energy around 1.91 eV (650 nm), any non-radiative decay via direct intersystem crossing to ^{3}LF followed by internal conversion through the LF manifold can be disregarded. Furthermore comparison between the emission spectra of **3** and **6** and the absorption spectra of **4** and **5** (see Figure S20a-b) reveals that singlet energy transfer from the porphyrin toward the Ru(II) endgroup is not relevant.[30, 43] In contrast, the available CV data suggests that hole-transfer to a ruthenium-based MO leading to a $\pi^*_{Por}\leftarrow d_{Ru}$ singlet MLCT state will constitute a quite likely process, as previously stated for the closely related dyad **C**.[7] Interestingly, the TD-DFT calculations on $\mathbf{1}^5$ and **2** fail to identify this charge-separated (CS) state among the first ones computed, in line with a forbidden or poorly allowed vertical

transition to this state from the ground state (GS). As a result, this excited state which overlaps with the first Q-bands in **1** and **2**, is difficult to detect experimentally.

Mono-cations. For Ru(III) complexes, the existence of (forbidden) low-lying doublet ligand field (LF) states has been previously established,[13, 23] making internal conversion via ^{2}LF states a potential new contributor for non-radiative deactivation. Then, comparison of the emission spectra of **6** and **3** and of the absorption spectra of $\mathbf{5}^+$ and $\mathbf{4}^+$ indicates some overlap (Figures S20a-b), making energy transfer from porphyrin core to the Ru(III) complex another potential contributor for non-radiative deactivation. The low extinction coefficient of the LMCT excited state of the Ru(III) complex will result in a very small overlap. This process might therefore not be a dominant one for trapping the fluorescence. Here again, based on the available redox data, a hole-transfer process to porphyrin- or to aryl-based MOs and leading to the formation of singlet $d_{Ru}\leftarrow\pi_{Por}$ or $d_{Ru}\leftarrow\pi_{Ar}$ LMCT (CT) states constitutes a likely alternative. LMCT states can be experimentally detected on the spectra of $\mathbf{1}^+$ and $\mathbf{2}^+$ and the Marcus-type analysis of the electron-transfer parameters suggest that the quenching process forming such LMCT states could be of comparable efficiency as the redox-trapping process occurring for the neutral compounds, in spite of its much larger exergonicity.[43]

Di-cations. From our SEC data (Figure S13),[5] both the porphyrin core and the ruthenium alkynyl endgroup appear to be mono-oxidized in the dications $\mathbf{1}^{2+}$ and $\mathbf{2}^{2+}$. Thus, the porphyrin-based Q-states are now strongly modified in nature and energy. The absorption spectra of the reference compounds $\mathbf{3}^+$ and $\mathbf{6}^+$ reveal a single red-shifted Q-band with much higher extinction coefficients than for **3** and **6**. Furthermore, in the dicationic dyads, this state significantly overlaps with the LMCT absorption of the Ru(III) fragments modelled by $\mathbf{5}^+$ and $\mathbf{4}^+$ (Figure S20), potentially leading to a much more efficient energy transfer than for $\mathbf{1}^+$ and $\mathbf{2}^+$. In this respect, the failure to detect any emission at such wavelengths during the spectrofluorometric experiments suggests that the dications $\mathbf{1}^{2+}$ and $\mathbf{2}^{2+}$ are totally non-emissive in the spectral range investigated.[46-48] In addition, such diradical compounds will also present a manifold of different CS states with various spin multiplicities at low energy providing many additional pathways for non-radiative deactivation. According to Figure 6, these species, while presenting the most contrasted fluorescence-switching relative to the neutral dyads, are also much more chemically reactive than the previous redox parents.

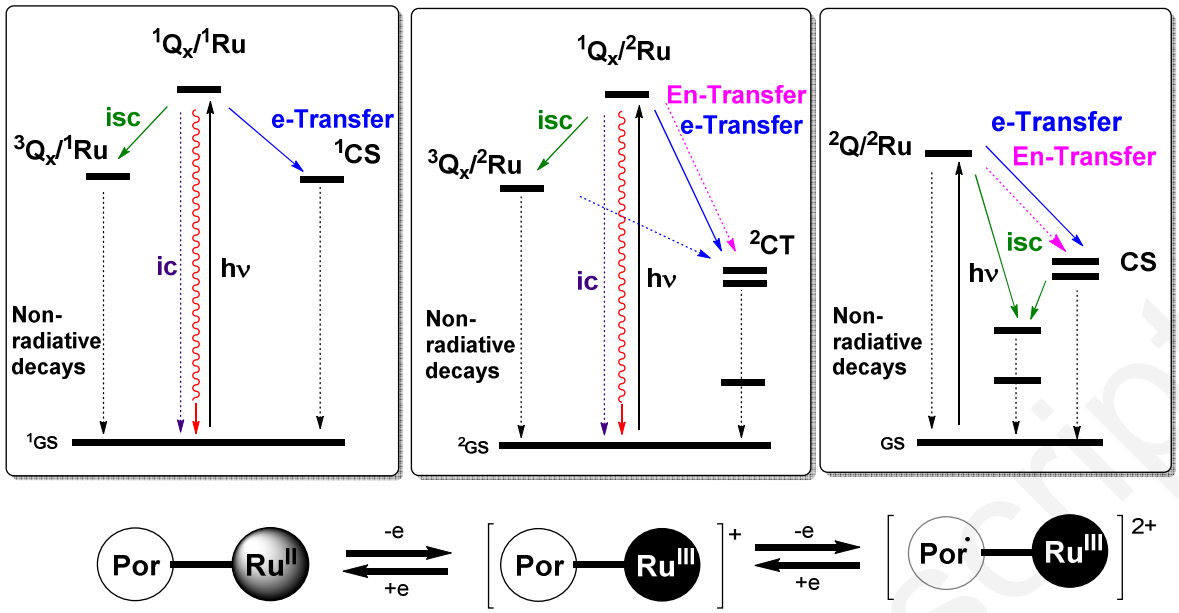

Figure 8. Main photophysical processes determining the luminescence (in red) of the dyads **1** and **2** in each redox state (ic: internal conversion, isc: intersystem crossing, e: electron, En: energy). For the monocation, the electron transfers from the triplet state are also indicated.

Redox Switching for 1 and 2

In spite of the low luminescence quantum yields found for the dyads **1** and **2** and the fact that the oxidized states are even less luminescent, we show that the redox-control of their emission can still lead to a sizable change in their luminescence (Figure 6), a more contrasted behavior being obtained for the dyad **1** in this respect. Similarly to what had been found previously for the dyad **C** (Figure 1), the porphyrin-based emissive state experiences distinct redox-quenching processes of fairly comparable efficiencies in its neutral and mono-cationic redox state. As a result, these photoinduced electron-transfer processes strongly quench the fluorescence of the dyads compared to porphyrin not functionalized with redox-active metal-alkynyl endgroups such as **3** or **6**. In contrast to the former investigations on these systems,[7] we stress here that driving forces (ΔG_{eT} or $\Delta G_{eT'}$) derived from Rehm-Weller considerations are not sufficient alone to draw conclusions about the relative efficiency of the redox-trapping processes occurring in distinct redox states, but that activation energies ($\Delta G^{\neq}$) should actually be considered instead. Indeed, for the electron transfer taking place in the mono-oxidized state of these dyads, the process is strongly exergonic and takes place in the inverted Marcus region.[43] As a consequence, larger driving forces actually result in slower kinetics. Taken at

face value, our data (Tables 2 and 3) indicate that, provided the electronic coupling for electron-transfer (H_{ab}) does not change much between the neutral dyad and their monocations, redox-quenching will be more efficient in the latter case, in line with experimental observations. This suggests that the fluorescence switching presently observed for **1** and **2** subsequent to mono-oxidation might be essentially determined by the redox-trapping reactions. Pushing the oxidation further reinforces this switching, given that fully non-emissive dications are apparently formed at higher oxidation potentials, but at the cost of a lower electrochemical reversibility (Figure 8).[49] However, we also show that both dyads can undergo energy transfer only in their mono-oxidized state, which provides another potential explanation for the observed luminescence modulation, a feature not previously envisioned for dyad **C**.

Coming back to the other systems (**A-C**) previously reported for redox-switching of fluorescence,[3, 4, 7] we can check if redox quenching also determines the fluorescence switching observed. Due to the strong structural similarities between **1-2** and **C**, it is not surprising that redox quenching influences the switching in a related way in **C** as in **1-2**.[7] However, can we also rationalize the different behavior observed for **A** and **B** based on redox-quenching in the excited state? From the available electrochemical and spectroscopic data and considering adapted reorganization energies,[3, 4] the answer seems positive (Tables S8 and S9). Indeed, contrary to **1** and **2**, the activation barrier for redox quenching appears higher in the oxidized state than in the neutral state for these systems, in line with the reported switching. This is not so surprising for **B**, which presents significantly different redox potentials due to the different porphyrin and Ru(II) alkynyl complex present in that dyad. This statement is more surprising for **A**, given the closeness of the redox potentials for mono-oxidation of ferrocene and of the [*trans*-Ru(η^2-dppe)$_2$(Cl)] alkynyl complex. Actually, the reason for this behavior mostly resides in the lower reorganization energy of ferrocene. Based on data published for relevant mixed-valent complexe, values closer to 0.6 eV should be considered.[50] This suggests that redox-quenching also controls the fluorescence switching observed upon oxidation in **A** and **B**. Notably, in the second case, this switching might also be strengthened/supplemented by a non-radiative decay process occurring via energy transfer in $\mathbf{B}^+$ preferably than in **B** (as judged from the overlap between the porphyrin-based emission

and the lower lying CT band in **B** *vs.* $\mathbf{B}^+$).[4] The thermodynamic parameters underlying redox quenching in a given redox state should therefore always be closely considered when designing redox-switchable luminophores (dyads) with related structures. As illustrated here *the efficiency of the redox quenching process does not solely rely on the Gibbs free energy (ΔG_{eT}) for the photo-induced charge transfer (PICT).*

Then, from a more practical standpoint, considering chemical stability issues with **1** and **2**, a strongly contrasted redox switching already after oxidation of the Ru(II) complex is desirable.[29] In this respect, dyad **2** performs less well than dyad **1** which features a shorter spacer between the ruthenium alkynyl complex and the porphyrin ring. From the literature, higher electronic couplings (H_{ab}) are expected to take place through a 1-ethynyl,4-phenylene[51] bridge than through a 2-ethynyl,7-fluorenyl one.[15] However, even when the switching process is solely controlled by redox trapping (*i.e.* dominant k_{eT} values in eq. 5), the contrast depends actually on the relative change in rate between the different electron-transfer processes occurring each in a distinct redox state for a given dyad *i.e.* on the $[(k_{eT})^{Neutral}/(k_{eT})^{Mono\text{-}Oxidized}]$ ratio. Based on eq. 4, this relative change depends on the *change* in coupling constants *and* in activation energies *between* two redox states *of the same compound*. From the activation energies presently derived (Tables 2 and 3), a better contrast can be predicted for **1** provided no change in the coupling constant of these dyads takes place upon oxidation, while a more pronounced increase in electronic coupling between **1** and $\mathbf{1}^+$ than between **2** and $\mathbf{2}^+$ would reinforce this difference (and *vice-versa*). More generally, considering the counteracting influences exerted on the electron transfer kinetics by a change in the spacer (via H_{ab} and $\Delta G^{\neq}$), when progressing from **1** to **2** (or from $\mathbf{1}^+$ to $\mathbf{2}^+$), it appears that the impact on fluorescence of seemingly simple structural modifications brought to such organometallic dyads cannot be predicted without modelling *a minima* the electron-transfer, stressing the need to gather accurate information about electronic couplings, redox potentials and reorganization energies for the various building blocks composing these dyads.[13]

Conclusions

The new organometallic dyad **2**, combining the highly luminescent tetrafluorenylporphyrin

core with one redox-active [*trans*-Ru(dppe)$_2$Cl(C≡C-)] ruthenium fragment was synthesized. Data from SEC absorption spectroscopy and calculations indicate that the porphyrin unit is a spectator group during the oxidation, even more for **2** than for **1**, pointing to a reduced electronic coupling with the organometallic endgroup through the extended bridge in **2**.

The electrofluorochromic behavior of this new compound and that of its previously published trifluorenylphenylporphyrin analogue **1** were then probed. The fluorescence of these dyads is (partly) quenched upon oxidation, but **2** exhibits a far less contrasted fluorescence-switching than **1**. Pushing the oxidation to higher potentials leads to a larger switching in both cases, but also to a lower chemical reversibility. For both dyads in the neutral state, the existence of a metal-to-ligand charge transfer (MLCT) states at low energy, "hidden" under the Q bands, was established. These states efficiently quench the porphyrin-based fluorescence in their neutral state. Upon mono-oxidation, low-lying ligand-to-metal charge transfer (LMCT) states are formed which can also quench the fluorescence efficiently in their oxidized states. Thus, the way the redox-switching operates in these dyads depends on the relative rates of these photo-induced electron-transfer occurring in each redox state and on their interplay with additional (non-radiative) decay processes which might be "turned on" or "turned off" by oxidation, such as energy-transfer or internal conversion. For **1** and **2**, based on data from cyclic voltammetry and accordingly with what was experimentally observed, a faster redox-quenching is predicted to take place in the mono-oxidized state, while this redox-quenching process is possibly also supplemented by an energy-transfer process in the monocations $\mathbf{1}^+$ and $\mathbf{2}^+$.

Experimental section

General procedures

All reactions were performed under argon and were magnetically stirred. Solvents were distilled from appropriate drying agent prior to use, DCM and $CHCl_3$ from CaH_2 and THF was distilled using sodium/benzophenone system.[49] Other solvents used were of HPLC grade. Commercially available reagents were used without further purification unless otherwise stated. Pyrrole and 2-fluorenecarboxaldehyde were purchased from Aldrich and were used as

received. ^{1}H and $^{31}P\{^{1}H\}$ spectra were recorded on BRUKER Ascend 400 and 500 at 298K. High-resolution mass spectra were recorded on different spectrometers: a Bruker MicrOTOF-Q II, a Thermo Fisher Scientific Q-Exactive in ESI positive mode and a Bruker Ultraflex III MALDI Spectrometer at CRMPO (Centre Regional de Mesures Physiques de l'Ouest) in Rennes.

Synthesis of the organometallic porphyrin 2

In a Schlenk tube, a mixture of the organic porphyrin (**3**) (40 mg, 0.03 mmol, 1 equiv), ruthenium(II) complex (33 mg, 0.03 mmol, 1.1 equiv) and $NaPF_6$ (5.0 mg, 0.1 mmol, 1 equiv) were stirred in distilled dichloromethane under argon at room temperature. The reaction medium was degassed by argon bubbling for 10 min. Then the system was kept stirring for 96 h at room temperature in dark. Finally, NEt_3 was injected to complete the reaction. After evaporation of the volatiles, the residue was purified by basic Al_2O_3 chromatography using CH_2Cl_2/NEt_3 (100:1) as eluent; the dark violet powder was isolated to gain 42 mg of pure **2** (63% yield). ^{1}H NMR (400 MHz, $CDCl_3$, ppm), see Figure 2 for attribution : δ = 8.96-8.93 (m, 8H, $H_{\beta\text{-pyrrolic}}$), 8.26-8.15 (m, 8H, $H_{fluorenyl}$), 8.10-8.08 (m, 4H, $H_{fluorenyl}$), 7.97 (d, 4H, J = 6.0 Hz, $H_{fluorenyl}$), 7.70 (d, 1H, J = 7.6 Hz, $H_{fluorenyl}$), 7.59-7.58 (m, 7H, $H_{fluorenyl}$, $H_{Ph\text{-}dppe}$), 7.50-7.42 (m, 11H, $H_{fluorenyl}$, $H_{Ph\text{-}dppe}$), 7.35-7.33 (m, 8H, $H_{fluorenyl}$, $H_{Ph\text{-}dppe}$), 7.21 (t, J = 7.0 Hz, 8H, $H_{Ph\text{-}dppe}$), 7.05-6.99 (m, 14H, $H_{Ph\text{-}dppe}$), 6.79 (d, 2H, J = 7.6 Hz, $H_{Ph\text{-}dppe}$), 2.75 (s, 8H, $H_{CH2\text{-}dppe}$), 2.15 (s, 16H, H_a), 1.22-1.15 (m, 16H, H_c), 0.90-0.84 (m, 16H, H_b), 0.82-0.70 (m, 24H, H_d), -2.56 (m, 2H, NH). $^{31}P\{^{1}H\}$ NMR (160 MHz, $CDCl_3$, ppm): δ = 49.4 (s, 4P, $(dppe)_2$). UV-vis (λ_{max}[ε / 10^3 $M^{-1}cm^{-1}$], CH_2Cl_2, nm): 262 [122], 310 [82], 365 [73], 427 [416], 520 [21], 559 [21], 593 [14], 649 [8]. HRMS-ESI for $C_{158}H_{157}N_4P_4RuCl$: m/z = 2371.0070 [$M^{+\bullet}$] (calcd: 2371.0085).

Spectroscopic Measurements

All photophysical properties have been performed with freshly-prepared air-equilibrated solutions at room temperature (298 K). UV-Vis absorption spectra were recorded on a BIO-TEK instrument UVIKON XL spectrometer or on a Jasco V-570 spectrophotometer. PL emission was recorded on a Photon Technology International (PTI) apparatus coupled on an 814 Photomultiplier Detection System, Lamp Power Supply 220B and MD-5020. Steady-state fluorescence measurements were performed at room temperature (R. T.) on dilute solutions (*ca.* 10^{-6} M, optical density < 0.1) contained in standard 1 cm quartz cuvettes using an Edinburgh Instrument (FLS920) spectrometer in photon-counting mode, equipped with a

calibrated quantum counter for excitation correction. Fully corrected emission spectra were obtained, for each compound, after excitation at the wavelength of the absorption maximum, with $A_{\lambda ex} < 0.1$ to minimize internal absorption. Fluorescence quantum yields were measured using standard methods; TPP in CH_2Cl_2 (Φ_{lum} = 0.12 at λ_{ex} = 417 nm) was used as a reference. The reported fluorescence quantum yields are within ± 10%.

Electrochemistry

Cyclic voltammograms were recorded with an Autolab PG-STAT 30 potentiostat at 20 °C from solutions of ca. 10^{-4} M analyte in dry dichloromethane containing 0.1 M $[Bu_4N][PF_6]$ at scan rate v = 100 $mV.s^{-1}$ under a dry nitrogen atmosphere. The single-compartment three-electrode cell was equipped with platinum wire counter and reference electrodes and a glassy carbon working electrode. Redox potentials are reported with the decamethylferrocene/decamethylferrocenium ($Cp^*_2Fe^+/Cp^*_2Fe$) redox couple used as an internal reference system at -0.53 V[50] vs the usual ferrocene/ferrocenium (Cp_2Fe^+/Cp_2Fe) redox couple at 0.0 V in CH_2Cl_2.

Spectroelectrochemistry

Spectroelectrochemical (SEC) experiments were performed at room temperature in an airtight optically transparent thin-layer electrochemical (OTTLE) cell[51] equipped with Pt minigrid working and counter electrodes (32 wires cm^{-1}), Ag wire pseudo-reference electrode and CaF_2 windows for a 200 μm path-length solvent compartment. CH_2Cl_2 solutions containing 0.1 M $[Bu_4N][PF_6]$ electrolyte were used in the cell for SEC experiments. The cell was fitted into the sample compartment of a Cary UV-Vis-IR spectrophotometer or a Nicolet Avatar 6700 FT-IR spectrometer. Bulk electrolysis was carried out using an Autolab PG-STAT 30 potentiostat.

Computations

All computations were carried out with the Gaussian 09 package.[55] The S_0 model geometries of **1′** and **2′** with no symmetry constraints were fully optimized with the B3LYP and CAM-B3LYP functionals[56,57,58] using the 3-21G* basis set[59,60] for all atoms. The 3-21G* basis set is used here as it has been shown to be suitable for ruthenium acetylides elsewhere.[61,62,63,64,65,66,67] Computed absorption data were obtained from TD-DFT calculations on i) B3LYP/3-21G* optimized S_0 geometries at B3LYP/3-21G* with an energy

scaling factor of 0.92 applied to calculated transition energies for direct comparison with experimental data and ii) CAM-B3LYP/3-21G* optimized S_0 geometries at CAM-B3LYP/3-21G* with an energy scaling factor of 0.85 applied to calculated transition energies for direct comparison with experimental data. The MO diagrams in Figures 4 and S14-S15 were generated with the Gabedit package[68] and the %MO contributions in Tables S3, S5 and S6 were obtained using the GaussSum software.[69] Results from CAM-B3LYP computations are discussed in the electronic supporting information (Figures S14-S16 and Tables S5-S7).

Electrofluorochromism

The voltafluorogram of 1 was recorded in a thin layer spectroelectrochemical cell[51] with Pt minigrid, Pt wire and Ag wire as working, auxiliary and pseudo-reference electrodes respectively in CH_2Cl_2/[NBu_4][PF_6] (0.1 M). The cell is connected to a spectrofluorimeter (FluoroLog 3, Horiba) through optical fibers and to a potentiostat (CH Instruments 600).

Chronofluorograms of **1** and **2** are recorded in a homemade electrochemical cell made by sticking a glass vial on an ITO coated microscope glass slide used as the working electrode. A Pt wire and Ag wire are used as counter and pseudo-reference electrodes respectively. The cell is put on the stage of an inverted fluorescence microscope (Nikon TI-U) equipped with a ×40 large numerical aperture objective. Fluorescence measurements are performed with an excitation bandpass filter centered at 447 nm (BP447), a dichroic mirror (FITC 506 nm) and an emission filter (AELP 520 nm). The set-up is similar to the one used in ref.[70]

ACKNOWLEDGEMENTS

The authors acknowledge CNRS for their financial support and China Scholarship Council (CSC) for PhD funding (XZ and LS) as well as "the Ministère de l'Enseignement Supérieur et de la Recherche Scientifique de Tunisie" for PhD funding (SA). We also thank CNRS and Durham University for supporting the Rennes-Durham collaboration.

REFERENCES AND NOTES

1. M. R. Wasielewski, *J. Org. Chem.*, 2006, **71**, 5051-5066.
2. G. McDermott, S. M. Prince, A. A. Freer, A. M. Hawthornthwaite-Lawless, M. Z. Papiz, R. J. Cogdell and N. W. Isaacs, *Nature*, 1995, **374**, 517-521.
3. J. Rochford, A. D. Rooney and M. T. Pryce, *Inorg. Chem.*, 2007, **46**, 7247-7249.
4. M. Murai, M. Sugimoto and M. Akita, *Dalton Transactions*, 2013, **42**, 16108-16120.
5. A. Merhi, X. Zhang, D. Yao, S. Drouet, O. Mongin, F. Paul, J. A. G. Williams, M. A. Fox and C. O. Paul-Roth, *Dalton Trans.*, 2015, **44**, 9470-9485.
6. A. Merhi, G. Grelaud, N. Ripoche, A. Barlow, M. P. Cifuentes, M. G. Humphrey, F. Paul and C. O. Paul-Roth, *Polyhedron*, 2015, **86**, 64-70.
7. L. Norel, C. Tourbillon, J. Warnan, J.-F. Audibert, Y. Pellegrin, F. Miomandre, F.Odobel and S. Rigaut, *Dalton Trans.*, 2018, **47**, 8364-8374.
8. F. Paul, B. J. Ellis, M. I. Bruce, L. Toupet, T. Roisnel, K. Costuas, J.-F. Halet and C. Lapinte, *Organometallics*, 2006, **25**, 649-665.
9. C. O. Paul-Roth, J. Rault-Berthelot, J. Letessier, G. Simonneaux and J.-F. Bergamini, *J. Electroanal. Chem.*, 2007, **606**, 103-116.
10. X. Zhang and C. O. Paul-Roth, *J. Porphyrins Phthalocyanines*, 2019, **23**, 185-195.
11. C. Poriel, Y. Ferrand, P. Le Maux, C. Paul-Roth, G. Simonneaux and J. Rault-Berthelot, *J. Electroanal. Chem.*, 2005, **583**, 92-103.
12. C. O. Paul-Roth, J. A. G. Williams, J. Letessier and G. Simonneaux, *Tetrahedron Lett.*, 2007, **48**, 4317-4322.
13. A. Triadon, G. Grelaud, N. Richy, O. Mongin, G. J. Moxey, I. M. Dixon, X. Yang, G. Wang, A. Barlow, J. Rault-Berthelot, M. P. Cifuentes, M. G. Humphrey and F. Paul, *Organometallics*, 2018, **35**, 2245-2262.
14. F. Malvolti, C. Rouxel, G. Grelaud, L. Toupet, T. Roisnel, X. Yang, G. Wang, A. Barlow, F. I. Abdul Razak, R. Stranger, M. P. Cifuentes, M. G. Humphrey, O. Mongin, M. Blanchard-Desce, C. O. Paul-Roth and F. Paul, *Eur. J. Inorg. Chem.*, 2016, 3868-3882.
15. F. Malvolti, C. Rouxel, A. Triadon, G. Grelaud, N. Richy, O. Mongin, M. Blanchard-Desce, L. Toupet, F. I. Abdul Razak, R. Stranger, M. Samoc, X. Yang, G. Wang, A.

Barlow, M. P. Cifuentes, M. G. Humphrey and F. Paul, *Organometallics*, 2015, **34**, 5418-5437.

16. D. Yao, X. Zhang, S. Abid and C. O. Paul-Roth, *J. Photochem. Photobiol. A*, 2017, **338**, 96-103.
17. S. Guesmi, D. Touchard and P. H. Dixneuf, *Chem. Commun.*, 1996, 2773-2774.
18. Accurate measurement of very low fluorescence quantum yields is problematic with **2**, since traces of non-metallated free base precursor **3** or related free bases might interfere.
19. C. O. Paul-Roth, J. Rault-Berthelot, G. Simonneaux, C. Poriel, M. Abdalilah and J. Letessier, *J. Electroanal. Chem.*, 2006, **597**, 19-27.
20. M. V. Sheridan, K. Lam and W. E. Geiger, *Angew. Chem. Int. Ed.* , 2013, **52**, 12897-12900.
21. C. E. Powell, M. P. Cifuentes, J. P. Morrall, R. Stranger, M. G. Humphrey, M. Samoc, B. Luther-Davies and G. A. Heath, *J. Am. Chem. Soc.*, 2003, **125**, 602-610.
22. N. Gauthier, N. Tchouar, F. Justaud, G. Argouarch, M. P. Cifuentes, L. Toupet, D. Touchard, J.-F. Halet, S. Rigaut, M. G. Humphrey, K. Costuas and F. Paul, *Organometallics*, 2009, **28**, 2253-2266.
23. C. O. Paul-Roth, J. Rault-Berthelot and G. Simonneaux, *Tetrahedron*, 2004, **60**, 12169-12175.
24. M. A. Fox, J. D. Farmer, R. L. Roberts, M. G. Humphrey and P. J. Low, *Organometallics*, 2009, **28**, 5266-5269.
25. The hybrid-DFT CAM-B3LYP functional, usually better suited for compounds exhibiting charge-transfers over long distances in their excited states,[26] was also applied to model molecules of **1′** and **2′**, but the results were counter-intuitive based on cyclic voltammetry data (see ESI).
26. L. Weber, D. Eickhoff, T. B. Marder, M. A. Fox, P. J. Low, A. D. Dwyer, D. J. Tozer, S. Schwedler, A. Brockhinke, H.-G. Stammler and B. Neumann, *Chem. Eur. J.*, 2012, **18**, 1369-1382.
27. Note that the CV is different than that of Figure S7a because the setup is different and that the potential values are different from those reported in Table 1 because the reference electrode is not the same.
28. In the dications $\mathbf{1}^{2+}$ and $\mathbf{2}^{2+}$, the porphyrin ring is mono-oxidized (*i.e.* direct electrofluorochromism). Thus, if luminescent, this compound should present a largely

different emission spectrum than the neutral and mono-oxidized parents $\mathbf{1}^{n+}$ and $\mathbf{2}^{n+}$ (n = 0, 1) in which the fluorophore is not oxidized.[29]

29. P. Audebert and F. Miomandre, *Chem. Sci.*, 2013, **4**, 575-584.
30. R. Giasson, E. J. Lee, X. Zbao and M. S. Wrighton, *J. Chem. Phys. C*, 1993, **97**, 2596-2601.
31. A. Weller, *Z.. Phys. Chem. N. F.*, 1982, **133**, 93-98.
32. R. A. Marcus and N. Sutin, *Biochim. Biophys. Acta*, 1985, **811**, 265-322.
33. D. Astruc, *Electron Transfer and Radical Processes in Transition-Metal Chemistry*, VCH Publishers, Inc., Cambridge, 1995.
34. In this equation, e is the electron charge, ε_0 is the dielectric constant in vacuum, ε is the relative dielectric constant and d is the distance between the positive and negative charges in the charge separated (CS) state. These ΔG_{CS} values are given by the difference between the metal-based oxidation potential and first reduction potential of the porphyrin (Supporting Information), corrected by the electrostatic term expected in the CS species.
35. In this equation, $\Delta G^{\neq}$ is the activation energy for the redox quenching reaction, which depends on the reorganization energy (λ) and the driving force of the electron transfer process (ΔG_{eT}).
36. N. Gauthier, C. Olivier, S. Rigaut, D. Touchard, T. Roisnel, M. G. Humphrey and F. Paul, *Organometallics*, 2008, **27**, 1063-1072.
37. A. Klein, O. Lavastre and J. Fiedler, *Organometallics*, 2006, **25**, 635-643.
38. S. Drouet, A. Merhi, G. Grelaud, M. P. Cifuentes, M. G. Humphrey, K. Matczyszyn, M. Samoc, L. Toupet, C. O. Paul-Roth and F. Paul, *New J. Chem.*, 2012, **36**, 2192-2195.
39. The redox-trapping in the monocations $\mathbf{1}^+$ and $\mathbf{2}^+$ forms a LMCT state noted CT in Scheme 2B. From previous studies on Ru(III) alkynyl complexes such as $\mathbf{4}^+$ or $\mathbf{5}^+$,[13] LMCT state(s) corresponding to the formal transfer of one electron from the arylalkynyl (and not from the porphyrin) ring to the Ru(III) center are usually observed. UV-vis data (Figure S8) suggest the presence of such states for $\mathbf{1}^+$ and $\mathbf{2}^+$ (overlapping perhaps the CT state not clearly observed elsewhere). Redox-trapping of the Q_x state into these states constitute alternative trapping processes that could also take place with comparable efficiencies.

40. In this equation, k_{eT} is the electron-transfer rate, $\Delta G^{\neq}$ is the activation energy for the electron-transfer, k_B is the Boltzmann constant and T the temperature, whereas $C = (\pi/\hbar^2 k_B T\lambda)^{1/2}$ is presently a constant term for the dyads $\mathbf{1}^{n+}$ and $\mathbf{2}^{n+}$ (n = 0, 1). H_{ab} is the electronic coupling between the redox-active sites a and b, exchanging the electron.
41. The reorganization energies (λ) are estimates, while driving forces (ΔG_{eT}) suffer from experimental uncertainties on the redox potentials. The reorganization energies should actually be slightly different between $\mathbf{1}^{n+}$ and $\mathbf{2}^{n+}$ (n = 0, 1) and also between each redox state for the same compound.
42. With a reorganization energy of 0.8 eV, the activation barrier ($\Delta G^{\neq}$) for the trapping reaction into CT state with **1**[PF_6] and **2**[PF_6] becomes higher than for the trapping reaction of **1** and **2** into CS (0.097 and 0.074 vs. 0.061 and 0.056 eV, respectively).
43. E. S. Schmidt, T. S. Calderwood and T. C. Bruice, *Inorg. Chem.*, 1986, **25**, 3718-3720.
44. Considering a porphyrin-based triplet state 0.5 V lower in energy than the luminescent singlet Q_x state (which roughly corresponds to the T_2 states calculated for **1'** and **2'**, see DFT section),[43] activation energies of 0.5 and 1.0 meV and driving forces of -0.86 and -0.79 eV, respectively, are found.
45. F. Odobel, S. Suresh, E. Blart, Y. Nicolas, J.-P. Quintard, P. Janvier, J.-Y. Le Questel, B. Illien, D. Rondeau, P. Richomme, T. Häupl, S. Wallin and L. Hammarström, *Chem. Eur. J.*, 2002, **8**, 3027-3046.
46. We are not aware of reported luminescence for cationic porphyrins such as $\mathbf{6}^{+}$ and $\mathbf{3}^{+}$ in the literature.[47,48]
47. J. Fajer, D. C. Borg, A. Forman, D. Dolphin and R. H. Felton, *J. Am. Chem. Soc.*, 1970, **92**, 3451-3459.
48. A. Wolberg and J. Manassen, *J. Am. Chem. Soc.*, 1970, **92**, 2982-2991.
49. In this respect, the fact that redox-switching at 1.5 V does not shut off fluorescence reveals that total conversion of the sample into these dications is never reached in the spectro-electrochemical cell used for fluorescence measurements.
50. A. C. Ribou, J. P. Launay, M. L. Sachtleben, H. Li and C. W. Spangler, *Inorg. Chem.*, 1996, **35**, 3735-3740.
51. S. Ibn Ghazala, F. Paul, L. Toupet, T. Roisnel, P. Hapiot and C. Lapinte, *J. Am. Chem. Soc.*, 2006, **128**, 2463-2476.
52. D. D. Perrin and W. L. F. Armarego, *Purification of Laboratory Chemicals*, Pergamon Press, Oxford, 1988.

53. M. A. Fox, J. E. Harris, S. Heider, V. Pérez-Gregorio, M. E. Zakrzewska, J. D. Farmer, D. S. Yufit, J. A. K. Howard and P. J. Low, *J. Organomet. Chem.*, 2009, **694**, 2350-2358.
54. M. Krejcik, M. Danek and F. Hartl, *J. Electroanal. Chem.*, 1991, **317**, 179-187.
55. M. J. Frisch, G. W. Trucks, H. B. Schlegel, G. E. Scuseria, M. A. Robb, J. R. Cheeseman, G. Scalmani, V. Barone, B. Mennucci, G. A. Petersson, H. Nakatsuji, M. Caricato, X. Li, H. P. Hratchian, A. F. Izmaylov, J. Bloino, G. Zheng, J. L. Sonnenberg, M. Hada, M. Ehara, K. Toyota, R. Fukuda, J. Hasegawa, M. Ishida, T. Nakajima, Y. Honda, O. Kitao, H. Nakai, J. T. Vreven, J. A. Montgomery, J. E. Peralta, F. Ogliaro, M. Bearpark, J. J. Heyd, E. Brothers, K. N. Kudin, V. N. Staroverov, R. Kobayashi, J. Normand, K. Raghavachari, A. Rendell, J. C. Burant, S. S. Iyengar, J. Tomasi, M. Cossi, N. Rega, J. M. Millam, M. Klene, J. E. Knox, J. B. Cross, V. Bakken, C. Adamo, J. Jaramillo, R. Gomperts, R. E. Stratmann, O. Yazyev, A. J. Austin, R. Cammi, C. Pomelli, J. W. Ochterski, R. L. Martin, K. Morokuma, V. G. Zakrzewski, G. A. Voth, P. Salvador, J. J. Dannenberg, S. Dapprich, A. D. Daniels, O. Farkas, J. B. Foresman, J. V. Ortiz, J. Cioslowski and D. J. Fox, ed. I. Gaussian, Wallingford CT, 2009.
56. A. D. Becke, *J. Chem. Phys.*, 1993, **98**, 5648-5652.
57. C. Lee, W. Yang and R. G. Parr, *Phys. Rev. B.*, 1988, **37**, 785.
58. T. Yanai, D. P. Tew and N. C. Handy, *Chem. Phys. Lett.*, 2004, **393**, 51-57.
59. G. A. Petersson and M. A. Al-Laham, *J. Chem. Phys.* , 1991, **94**, 6081-6090.
60. G. A. Petersson, A. Bennett, T. G. Tensfeldt, M. A. Al-Laham, W. A. Shirley and J. Mantzaris, *J. Chem. Phys.* , 1988, **89**, 2193-2218.
61. M.-C. Oerthel, D. S. Yufit, M. A. Fox, M. R. Bryce and P. J. Low, *Organometallics*, 2015, **34**, 2395-2405.
62. M. A. Fox, B. Le Guennic, R. L. Roberts, D. A. Brue, D. S. Yufit, J. A. K. Howard, G. Manca, J.-F. Halet, F. Hartl and P. J. Low, *J. Am Chem. Soc.*, 2011, **133**, 18433-18446.
63. M. I. Bruce, A. Burgun, M. A. Fox, M. Jevric, P. J. Low, B. K. Nicholson, C. R. Parker, B. W. Skelton, A. H. White and N. N. Zaitseva, *Organometallics*, 2013, **32**, 3286-3299.
64. M. I. Bruce, M. A. Fox, P. J. Low, B. K. Nicholson, C. R. Parker, W. C. Patalinghug, B. W. Skelton and A. H. White, *Organometallics*, 2012, **31**, 2639-2657.
65. D. J. Armitt, M. I. Bruce, M. Gaudio, N. N. Zaitseva, B. W. Skelton, A. H. White, B. Le Guennic, J.-F. Halet, M. A. Fox, R. L. Roberts, F. Hartl and P. J. Low, *Dalton Trans.*, 2008, 6763-6775.

66. M. A. Fox, R. L. Roberts, T. E. Baines, B. Le Guennic, J.-F. Halet, F. Hartl, D. S. Yufit, D. Albesa-Jove, J. A. K. Howard and P. J. Low, *J. Am. Chem. Soc.*, 2008, **130**, 3566-3578.
67. J.-L. Xia, W. Y. Man, X. Zhu, C. Zhang, G.-J. Jin, P. A. Schauer, M. A. Fox, J. Yin, G.-A. Yu, P. J. Low and S. H. Liu, *Organometallics*, 2012, **31**, 5321-5333.
68. R. Allouche, *J. Comp. Chem.*, 2011, **32**, 174-182.
69. N. M. O'Boyle, A. L. Tenderholt and K. M. Langner, *J. Comp. Chem.*, 2008, **29**, 839-845.
70. F. Miomandre, J. F. Audibert, Q. Zhou, P. Audebert, P. Martin and J. C. Lacroix, *Electrochim. Acta* 2013, **110**, 56-62.